Available online at www.sciencedirect.com

ScienceDirect

Ceramics International 39 (2013) 8815–8822

CERAMICS INTERNATIONAL

www.elsevier.com/locate/ceramint

Preparation of glass–ceramic glazes for fast firing applications by CaF_2 substitution with B_2O_3 in the $CaO–CaF_2–Al_2O_3–SiO_2$ system

S. Banijamali*

Ceramic Department, Materials & Energy Research Center, Alborz, Iran

Received 17 February 2013; received in revised form 18 April 2013; accepted 19 April 2013
Available online 3 May 2013

Abstract

The present work aims to obtain glass–ceramic glazes for floor tile applications. In this regard, CaF_2 was gradually replaced by B_2O_3 in the glass compositions belonging to the $CaO–CaF_2–Al_2O_3–SiO_2$ system. This substitution led to a noticeable decrease of crystallization peak temperatures and to an alteration of the crystallization trend. In the B_2O_3 bearing glazes, anorthite and gehlenite were identified as the major and minor crystalline phases, respectively. During concurrent crystallization and sintering based on the fast firing program, glass–ceramic glazes containing 9 weight parts of fluorine and 12 weight parts of boron oxide showed the most desirable sinterability. The optimized glass–ceramic glazes offered acceptable micro-hardness, whiteness and thermal expansion behavior after fast firing heat treatment.

Keywords: Glass–ceramic; Crystallization; Glaze

1. Introduction

Recently, a developing interest has been focused on glass–ceramic glazes which are compatible with fast firing technology commonly used in tile industry [1]. A glass–ceramic glaze comprises a homogeneous distribution of crystalline phases dispersed in a residual glass matrix [2]. Controlled crystallization process based on the fast firing program guarantees adequate crystallinity as well as sufficient flow-ability and maturing of the glass–ceramic glazes [1,3–5]. In comparison with traditional glazes, glass–ceramic ones present superior chemical durability and mechanical properties such as micro-hardness and abrasion resistance. Furthermore, formation of crystalline phases leads to the achievement of appropriate opacity and whiteness without using zircon, zirconium oxide and tin oxide as opacifiers. The growing costs of these materials necessitate fabrication of glass–ceramic glazes with improved properties [1].

In the light of superior properties of glass–ceramic glazes and possibility to reduce raw materials' costs, various glass–ceramic systems have been proposed for floor tile glaze applications. For this purpose, various glazes containing different crystalline phases like mullite, diopside, cordierite, gahnite, spinel, etc. have been investigated [6–13].

The present work reports the results concerning the substitution of CaF_2 by B_2O_3 in the $CaO–CaF_2–Al_2O_3–SiO_2$ glass–ceramic glazes. It should be noted that the glass–ceramic bodies of the prototype $CaO–CaF_2–Al_2O_3–SiO_2$ system had been suggested for unglazed floor tiles applications, previously [14]. Due to the high cost of fluorine (CaF_2) and general potential of boron oxide as a glaze constituent such as lowering thermal expansion and improving both mechanical strength and scratch resistance [15], CaF_2 was gradually replaced by B_2O_3 in the glaze compositions. Hence, the starting glass frits containing various amounts of CaF_2 and B_2O_3 were prepared. The relevant glazes were exposed to a crystallization heat treatment scheduled according to the fast firing program. Crystallization behavior and sinterability of specimens were evaluated throughout simultaneous sintering and crystallization process. The arising changes in crystallinity, micro-hardness, whiteness index and coefficient of thermal expansion as well as the microstructural features of the optimized glazes were also characterized.

*Tel.: +98 9122132080; fax: +98 2636201888.
E-mail address: banijamalis@yahoo.com

0272-8842/$ - see front matter © 2013 Elsevier Ltd and Techna Group S.r.l. All rights reserved.
http://dx.doi.org/10.1016/j.ceramint.2013.04.069

Table 1
Chemical composition of the initial glasses (weight ratio).

Composition	CaO	Al_2O_3	SiO_2	CaF_2	B_2O_3
F9	23.5	42.8	33.7	9	–
B3F6	23.5	42.8	33.7	6	3
B6F3	23.5	42.8	33.7	3	6
B9	23.5	42.8	33.7	–	9
B12	23.5	42.8	33.7	–	12

2. Experimental procedure

The studied glaze compositions, formulated with different amounts of CaF_2 and B_2O_3, are presented in Table 1. The starting raw materials were reagent-grade chemicals of calcium carbonate (Merck 2066), fluorine (Merck 2840), boric acid (Merck 160), aluminum hydroxide (Merck 1093) and silica (Setabran, purity > 99%). The homogeneous mixtures of glass batches were melted in alumina crucibles at 1450–1480 °C in an electric furnace for 3h followed by rapid quenching in cold water to obtain frits. All frits were dry milled in an agate mortar for 30 min to reach the mean particle size of 10 μm. Crystallization behavior of glass frits was monitored by a differential thermal analyzer (Polymer Laboratories, STA-1640). Each DTA run was carried out in air atmosphere with alumina reference sample, using a heating rate of 20 ° C/min. Crystalline phases precipitated during heat treatment were identified by X-ray diffractometer (Siemens D500) with Cu-*K*α radiation. The quantitative determination of the crystalline phases in the optimized glass–ceramic glazes was performed from X-ray diffraction data by using the Ohlberg and Strickler method as Eq. (1):

$$X_c = (I_g – I_x)/(I_g – I_b) \times 100 \quad (1)$$

In this equation, I_g, I_x and I_b are the XRD intensity scattered by the parent glass, the partially crystallized glass and a mechanical mixture of oxide powders having the same composition as the parent glass, respectively [16].

The sinterability of glass–ceramic specimens was evaluated during sintering at several temperatures up to 1210 °C. Thereof, glass frits were mixed by 0.1 wt% CMC (carboxy methyl cellulose) and uniaxially pressed under a pressure of 5 MPa to obtain loosely compacted glass pellets with 2 cm in diameter. To simulate the condition of fast firing program, the glass pellets were heat treated according to Fig. 1.

In order to confirm the complete maturing of the selected compositions as glazes, they were applied as glaze slips on a conventional floor tile support. Glaze slips comprised frit and kaolin with weight ratio of 93/7 were mixed by 0.1 wt% carboxy methyl cellulose as a binder, 0.3 wt% sodium tripolyphosphate as a dispersant and 35 wt% water in a planetary mill for 30 min. The glazed specimens were also heat treated according to Fig. 1. The Vickers micro-hardness was measured utilizing the indentation method [17]. This test was carried out by applying a 100 g f load of a diamond indenter (Akashi, MVK-H21) for 30 s.

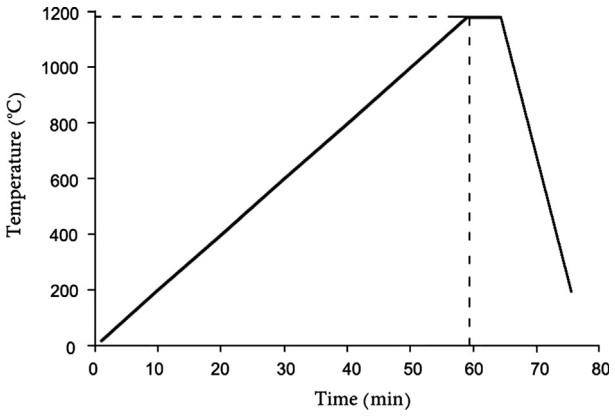

Fig. 1. Heat treatment regime scheduled according to the fast firing program.

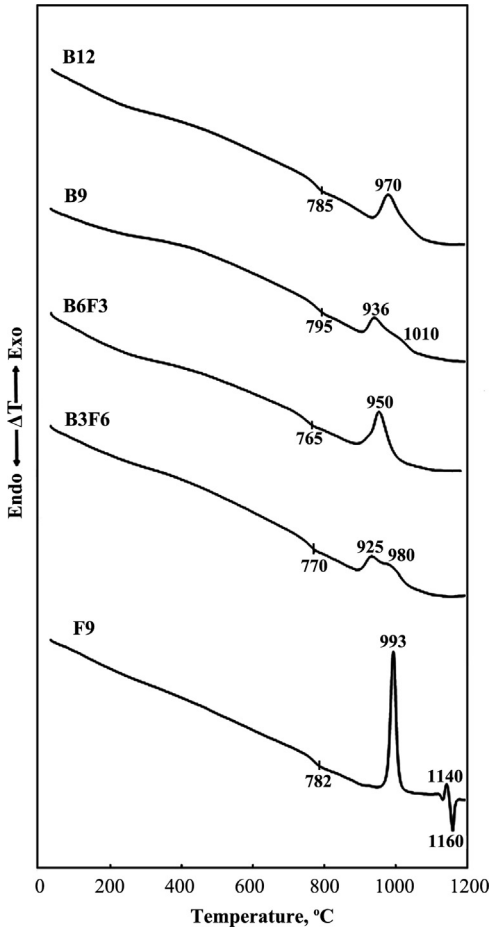

Fig. 2. DTA thermographs of glass particles (< 63 μm) at the heating rate of 20 °C/min.

To examine the consistency between thermal behavior of the glass–ceramic glazes and the support, thermal expansion coefficients of the most promising glazes and that of the support were measured by dilatometer (Netzsch 402E). This examination was performed at the heating rate of 10 °C/min in the temperature range of 25–300 °C. The prepared samples were rectangular bars with dimensions of 45 × 5 × 5 mm.

The coloring parameters (L^*, a^* and b^*) and whiteness index of the optimized glazes were calculated using GretagMacbeth

spectrophotometer (Color-Eye7000A) under illumination of three different sources of white light (D65, A and TL84). The gloss was also measured with a gloss meter (RohoPoint Novo Gloss IQ Goniophotometer) with a 60° light incident angle on the glaze surface.

The glazed samples after polishing and etching (in a 5 vol% HF solution for 20 s) were coated by a thin layer of gold and subjected to the SEM analysis (scanning electron microscope, Vega-Tescan). The SEM instrument was equipped with an energy dispersive analysis of X-ray (EDAX) capability.

3. Results and discussion

3.1. Differential thermal analysis

Fig. 2 shows the DTA thermographs of the glass particles. The DTA exothermic peaks correspond to crystallization. In the case of glass F9, a main sharp crystallization peak is located at 993 °C and the much smaller second peak can be observed at 1140 °C. In addition, an endothermic peak is obvious at 1160 °C which can be ascribed to the melting of a crystalline phase. In the DTA thermographs of other glasses, the intensity of crystallization peaks is noticeably lower than F9. Broadness of the crystallization peaks is also obvious especially for glasses B3F6 and B9. In the DTA thermographs of these glasses, a shoulder can be observed immediately after the main crystallization peak temperature (located at 980 and 1010 °C for B3F6 and B9, respectively). These shoulders were considered as the second crystallization peak temperature.

It is implied by Fig. 2 that the presence of B_2O_3 in the glass composition would decrease the dilatometric softening point temperature (T_s) of the glasses B3F6 and B6F3. Considering the similar role of B_2O_3 and CaF_2 as a flux in the structure of silicate glasses, simultaneous presence of them is expected to decrease the dilatometric softening point temperature of B3F6 and B6F3 rather than glass F9. On the other hand, complete elimination of CaF_2 from the glass composition leads to an increase in the dilatometric softening point temperature of glass B9. However, increasing the B_2O_3 content of glass B12 declined this temperature to 785 °C.

Table 2
Characteristic temperatures and crystalline phases developed at each sample.

Sample	Dilatometric softening point temperature (°C)	Crystallization temperatures (°C)	Crystalline phases
F9	782	993, 1140	W+A+C +G
B3F6	770	925, 980	A+G
B6F3	765	950	A+G
B9	795	936, 1010	A+G
B12	785	970	A+G

W: wollastonite, A: anorthite, C: calcium aluminum silicate, G: gehlenite.

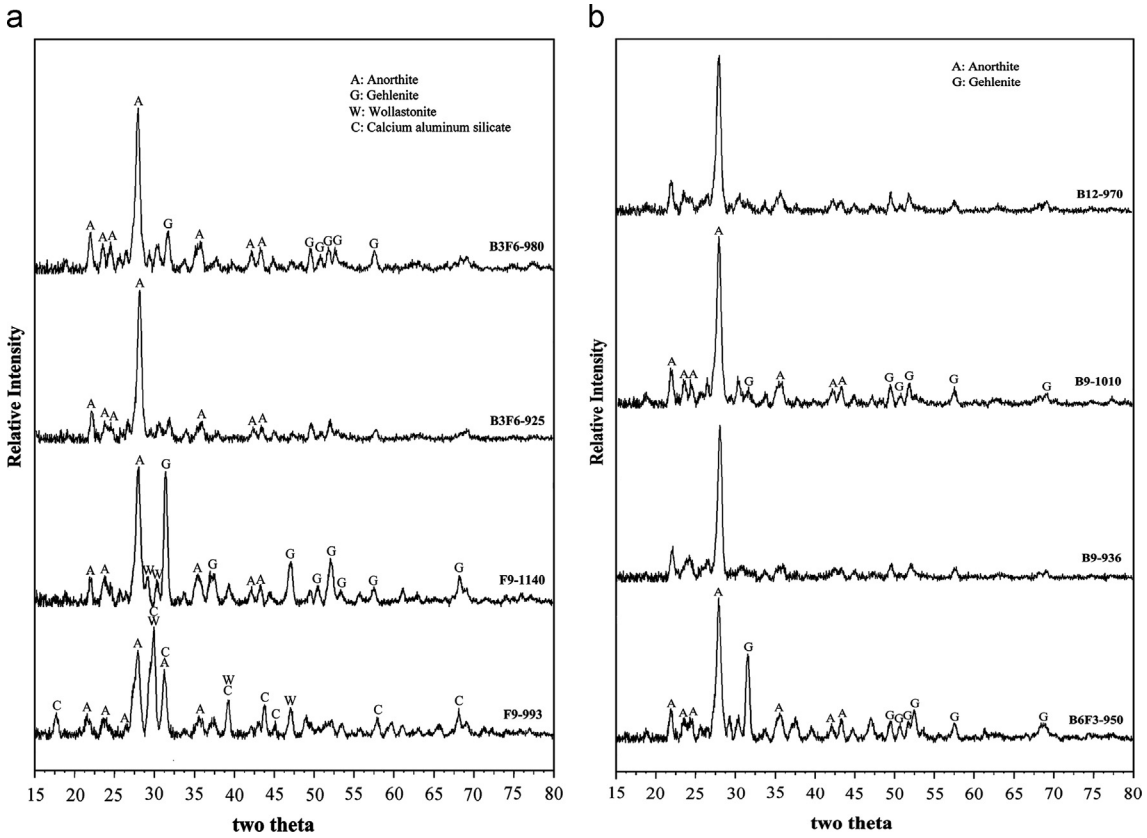

Fig. 3. (a) XRD patterns of the F9 and B3F6 glass particles heat treated for 5 min at the crystallization peak temperatures. (b) XRD patterns of the B6F3, B9 and B12 glass particles heat treated for 5 min at the crystallization peak temperatures.

3.2. X-ray diffraction analysis

In order to identify the crystalline phases precipitated through crystallization of the studied glasses, each glass frit was heat treated at its crystallization peak temperatures (extracted from the relevant DTA thermograph) for 5 min.

Fig. 3a and b depict the XRD patterns of the crystallized glass particles. As shown by Fig. 3a, three crystalline phases including wollastonite ($CaO \cdot SiO_2$), anorthite ($CaO \cdot Al_2O_3 \, 2SiO_2$) and calcium aluminum silicate ($CaO \cdot Al_2O_3 \cdot SiO_2$) are precipitated at the first crystallization peak of glass F9. Increasing temperature up to the second crystallization peak, results in the formation of gehlenite ($2CaO \cdot Al_2O_3 \cdot SiO_2$) whereas the intensity of wollastonite and calcium aluminum silicate is significantly decreased. Narrow temperature interval between the second crystallization peak and the endothermic peak of the relevant DTA graph suggests that two latter phases have been dissolved in the glass matrix.

According to Fig. 3a and b, B_2O_3 bearing glasses finally form anorthite as the dominant crystalline phase whereas peak lines of wollastonite and calcium aluminum silicate are not detectable. Gradual replacement of CaF_2 with B_2O_3 has reduced the CaO content in these specimens. As a result, the lower content of CaO can prevent crystallization of wollastonite and calcium aluminum silicate which have higher CaO content rather than anorthite.

Gehlenite was almost the minor crystalline phase in the B_2O_3 containing samples. However, the presence of gehlenite was much more evident in B6F3. Regarding the dilatometric softening point temperatures of the studied glasses, B6F3 has the lowest viscosity compared to other glasses. Presumably, the lowest viscosity of this glass has influenced the crystallization of gehlenite and improved it, kinetically.

In none of the B_2O_3 containing specimens, B_2O_3 has contributed into the crystalline structure. Thus, it can be concluded that it has mostly remained within the residual glass matrix. The DTA characteristic temperatures and the crystalline phases developed through the crystallization process have been summarized in Table 2.

3.3. Sinterability evaluation

In order to examine the sinterability of heat treated glass compacts, the water absorption and linear shrinkage of them were measured within the 1120–1210 °C temperature range (Fig. 4a and b). By increasing temperature, linear shrinkage of the sintered F9 and B12 was slightly increased to the maximum of 17–18%. Water absorption of specimens B3F6,

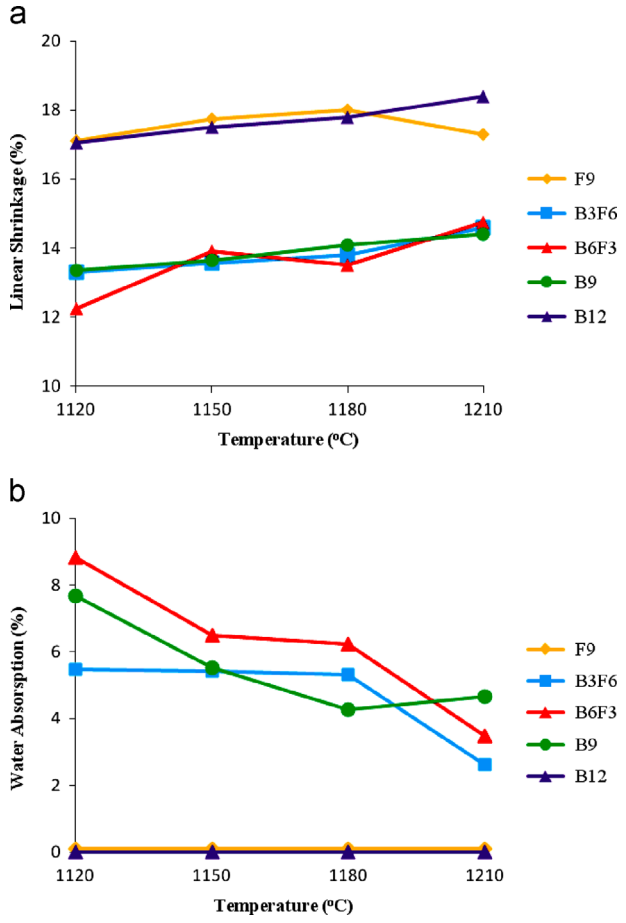

Fig. 4. (a) Variation of linear shrinkage versus sintering temperature. (b) Variation of water absorption versus sintering temperature.

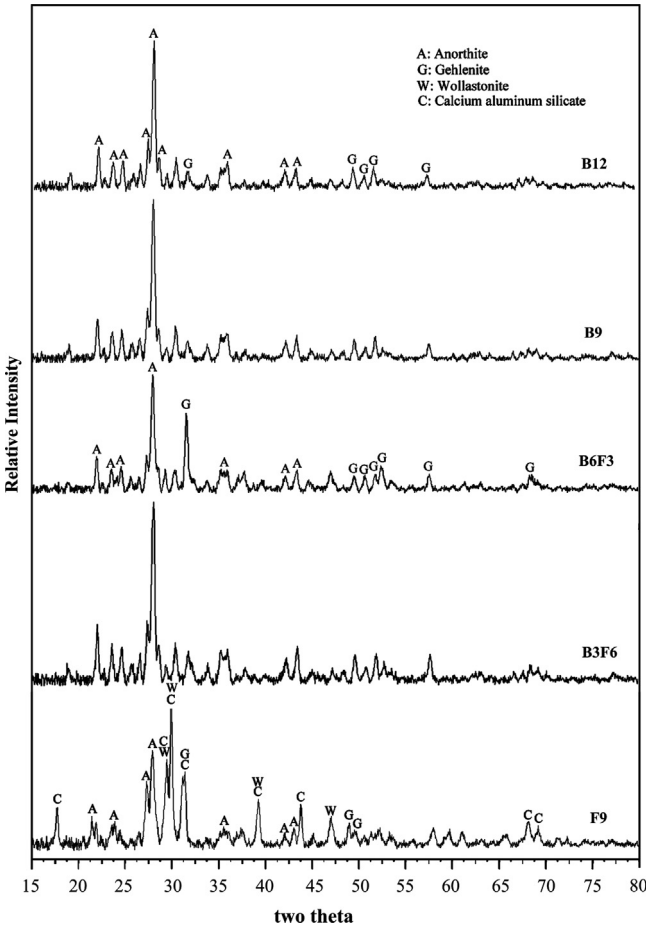

Fig. 5. Phase evolution of the glass–ceramic glazes heat treated at 1180 °C.

B6F3 and B9 was observed to reach the minimum amount of 3–5% at the end of the selected temperature range. However, water absorption of F9 and B12 remained equal to zero during sintering at various temperatures.

Based on the obtained results, the F9 and B12 samples appeared to have superior sinterability behavior. Their enhanced sinterability can be attributed to the increased viscous flow of the residual glass phase containing the higher amounts of CaF_2 and B_2O_3.

To facilitate a better understanding of the sinterability behavior, the temperature range between the dilatometric softening point (T_s) and crystallization peak (T_c) temperatures was measured for each glass. As reported by the literature, extending this temperature interval will postpone the crystallization process and improve the sinterability [18]. This interval was achieved to be 211, 155, 185, 141 and 185 °C for glasses F9, B3F6, B6F3, B9 and B12, respectively. This measurement confirms the better sinterability of glasses F9 and B12.

Since both F9 and B12 show appropriate sinterability at each sintering temperature and none of the other specimens reaches the full densification during the sintering step, 1180 °C was chosen as the optimized sintering temperature. This temperature was also selected to be in accordance with the maximum temperature commonly applied in the fast firing process.

As the next step, glaze slips were applied onto the pre-fired tile bodies following by heat treatment at 1180 °C. It can be inferred from the XRD patterns of the sintered glass–ceramic glazes (Fig. 5) that wollastonite, calcium aluminum silicate and anorthite are crystallized in the glaze F9. Due to the dissolution of wollastonite and calcium aluminum silicate in the glass matrix at 1160 °C, they are not expected to be observable. However, during cooling step and passing the 1160 °C peak temperature these phases have been re-crystallized in the glaze. In all B_2O_3 bearing glazes, anorthite and gehlenite were present as the major and minor crystalline phases, respectively. Concerning the better sinterability of F9 and B12, these compositions were considered as the most promising ones and consequently chosen for further examinations.

3.4. Characterization of the optimized glazes

Table 3 shows the crystallinity, micro-hardness and thermal expansion coefficients of the optimized glass–ceramic glazes (F9 and B12) sintered at 1180 °C. The crystallinity of the glazes measured through Ohlberg & Strickler method revealed that the glaze F9 has been more crystallized rather than B12. The amounts of the residual glass phase were obtained to be 26.8% and 38.6% for the glazes F9 and B12, in the same order.

Table 3
Crystallinity, micro-hardness and thermal expansion coefficient of the glazes.

Glaze	Crystallinity (%)	Vickers micro-hardness (VHN)	Coefficient of thermal expansion ($\times 10^{-6}$/°C)
F9	73.2	867.6	6.16
B12	61.4	676.4	5.11

Obviously, micro-hardness of the glaze F9 is considerably higher than that of the B12 one. More effective crystallization of various crystalline phases in the glaze F9 can be responsible for its higher micro-hardness. Furthermore, the presence of CaF_2 in the glaze F9 has increased the amount of CaO in the residual glass matrix which in turn reinforces the glass structural bonds. Hence, the glaze micro-hardness is not only affected by crystallinity but also is influenced by the hardness of the residual glass matrix.

Micro-hardness of a commercial zircon containing glaze was also determined to be compared with those of the optimized glazes. The VHN of the commercial glaze was found to be 589.5, considerably lower than the micro-hardness of the studied glazes. This measurement proves the effective role of crystallization in the improved micro-hardness of the glass–ceramic glazes.

The Dilatometry curves of the glazes and of the support have been illustrated in Fig. 6. Apparently, thermal expansion coefficients of both glazes are less than that of the support which results in the formation of compressive stress in the glaze matrix. Consequently, the crack propagation across the glaze will be restricted. From Fig. 6, the glass transition and dilatometric softening point temperatures of the residual glass phase were found to be 852 °C and 977 °C for the glaze B12; whilst the glass transition temperature of the glaze F9 was increased to 1104 °C and its softening point temperature was more than 1200 °C not

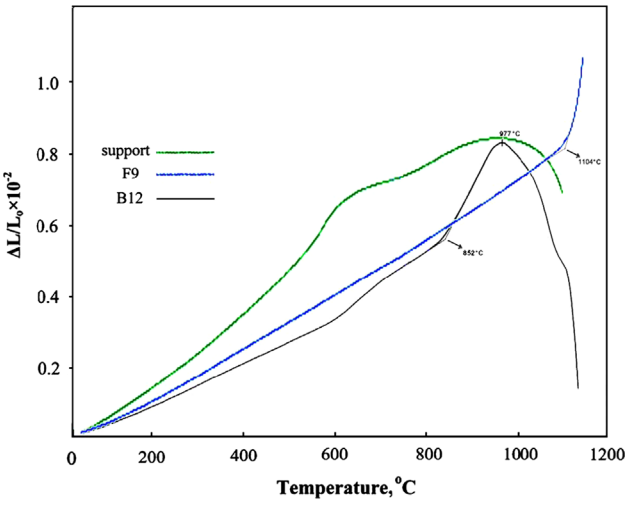

Fig. 6. Dilatometry curves of the glazes F9 and B12 at the heating rate of 10 °C/min.

Table 4
Coloring parameters (L^*, a^*, b^*), whiteness and gloss (60°) of the glazes.

Glaze	L^*	a^*	b^*	Whiteness index	gloss
F9	89.11	0.09	1.9	65.48	13.2
B12	87.57	0.15	1.23	65.3	15.4
GZ	91.23	−0.3	2.17	82.1	59.1

L^*, a^* and b^* have been reported as the average of three measurements under illumination of different sources of white light.

being detected in the measured temperature range. In brief, it can be concluded that the structural bonds of the residual glass phase of the glaze B12 are weaker compared with the glaze F9. This result is in agreement with the lower micro-hardness of the glaze B12.

Table 4 represents the results of colorimetry and gloss measurements of the studied glazes compared to a commercial zircon containing glaze (GZ). Close to 90% value of L^* and traces amounts of a^* and b^* reveal the tendency of both glass–ceramic glazes to the white color. The whiteness index of both was obtained around 65%. However, these glazes showed the lower whiteness relative to the commercial sample (GZ). Since the mentioned glazes had been applied onto the support without using an engobe layer, utilizing a suitable engobe would enhance their whiteness. On the other hand, the gloss measurements depicted a considerable difference between the glass–ceramic glazes and the commercial sample. Both glazes F9 and B12 had the lower gloss compared to the GZ. In fact, the effective formation of crystalline phases in these glazes declines their surface smoothness and conducts their appearance to the white matte status.

Microstructural study of the glaze F9 showed the presence of white needle like crystals (Fig. 7) which can be referred to the wollastonite crystalline phase [1,19] regarding their needle like morphology. However, the EDS analysis (Fig. 7c) showed some deviation from chemical composition of wollastonite, due to the small size of these crystals. Moreover, some grey pseudo spherical crystals are observable in the microstructure being ascribed to the formation of anorthite and calcium aluminum silicate phases.

Fig. 8 shows the SEM micrographs of the glaze B12. A homogeneous distribution of spherical crystals with dimensions less than 200 nm is detectable. The EDAX analysis of these crystals (Fig. 8c) showed the formation of a calcium aluminosilicate phase. With respect to the existence of anorthite as the dominant crystalline phase in this glaze, these crystals were attributed to anorthite.

4. Conclusions

Fast fired glass–ceramic glazes without zirconium content were obtained by gradual replacement of CaF_2 by B_2O_3 in the $CaO–CaF_2–Al_2O_3–SiO_2$ system. Elimination of CaF_2 from frit batches led to the formation of anorthite as the single crystalline phase in the B_2O_3 containing glazes. Among the studied glazes, utilizing 9 weight parts of CaF_2 (F9) and 12 weight

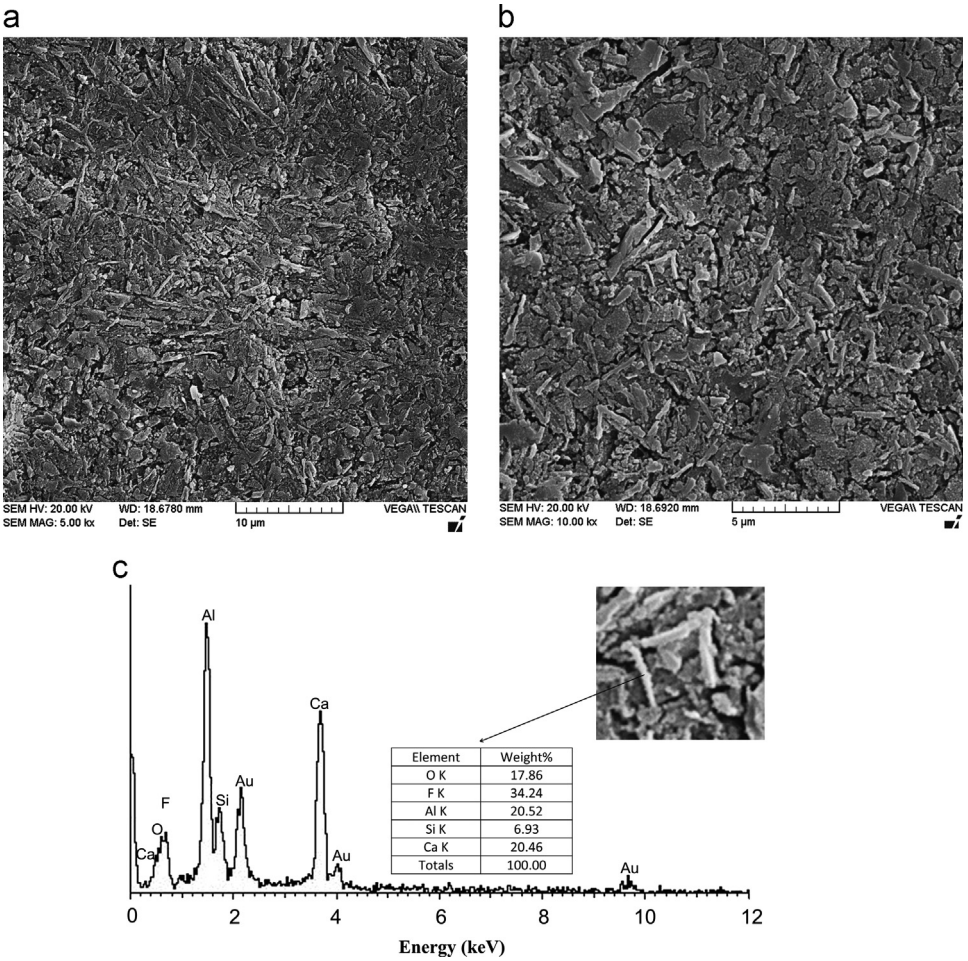

Fig. 7. SEM micrographs of the glass–ceramic glaze F9: (a) 5000 magnification, (b) 10,000 magnification, (c) EDAX pattern taken from the selected area (the amount of Au arising from gold coating was removed from the chemical analysis).

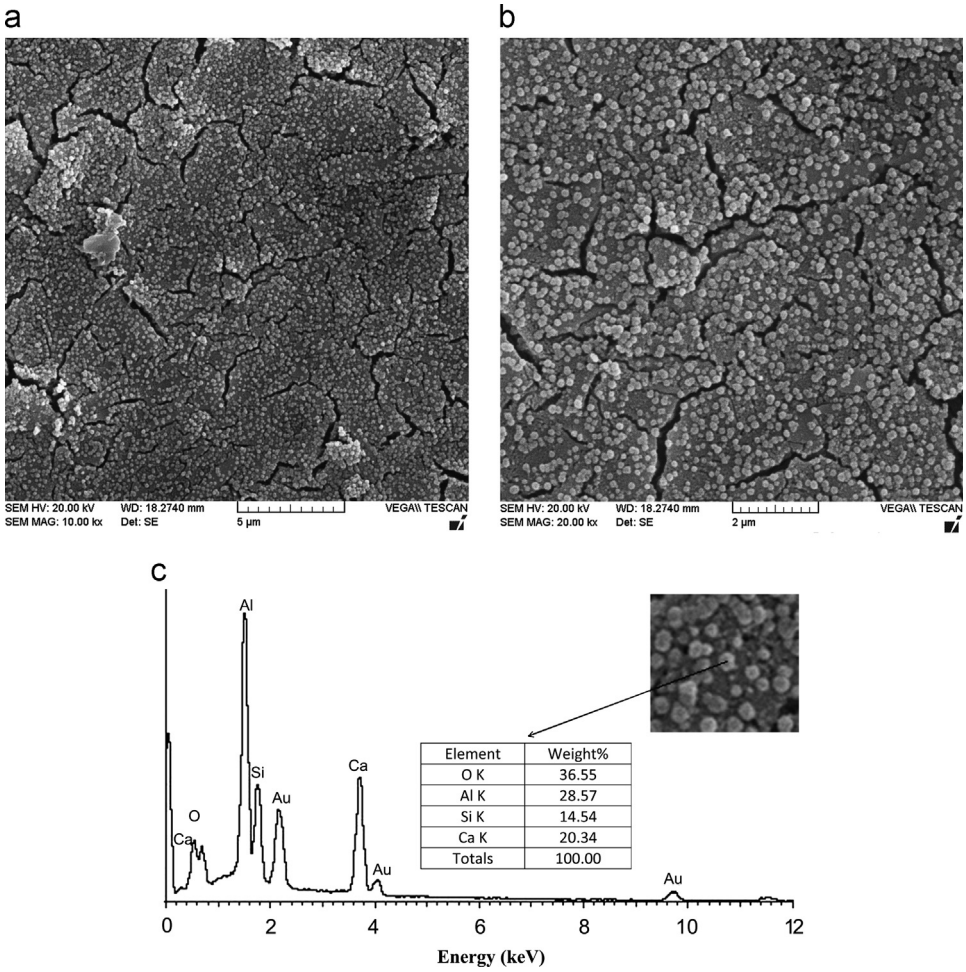

Fig. 8. SEM micrographs of the glass–ceramic glaze B12: (a) 10,000 magnification, (b) 20,000 magnification, (c) EDAX pattern taken from the selected area (the amount of Au arising from gold coating was removed from the chemical analysis).

parts of B_2O_3 (B12) offered the best sinterability. Although these glazes had different micro-hardness and crystallinity, both indicated appropriate consistency between their coefficients of thermal expansion and that of the support.

A comparison between the relevant glazes and a commercial floor tile glaze showed the higher micro-harness of glass–ceramic glazes. According to the colorimetry analysis, considerable whiteness was achieved by contribution of the crystalline phases to the opacity and whiteness of the glass–ceramic glazes. However, the gloss of these glazes was naturally decreased compared with the commercial sample due to the effective crystallization process giving them a white matte appearance.

Based on the obtained results, the optimized glass–ceramic glazes (F9 and B12) could be suitable choices for fast firing applications due to their zircon free composition, suitable sinterability, superior micro-hardness and considerable whiteness.

References

[1] R. Casasola, J. Ma Rincon, M. Romero, Glass–ceramic glazes for ceramic tiles: a review, Journal of Materials Science 47 (2012) 553–582.
[2] Z. Strnad, Glass–Ceramic Materials, Elsevier Science Publishers Amsterdam 9.
[3] T. Manfredini, Ceramic tile glazes: design, trends and application, in: 7th Conference of the European Ceramic Society, 2001, pp. 2031–2034.
[4] L. Barbieri, C. Leonelli, T. Manfredini, Technology and product requirements for fast firing glass–ceramic glazes, Ceramic Engineering and Science Proceedings 17 (1996) 11–22.
[5] A. Amoros, J.L. Bruni, F. Cariaati, J.E. Navarro, Glass–ceramic systems for super fast firing technologies, Industrial Ceramics 11 (1991) 7–10.
[6] F.J. Torres, E.R. de Sola, J. Alarcon, Effect of boron oxide on the microstructure of mullite-based glass–ceramic glazes in the CaO–MgO–Al_2O_3–SiO_2 system, Journal of the European Ceramic Society 26 (2006) 1185–1192.
[7] F.J. Torres, E.R. de Sola, J. Mechanism of crystallization of fast fired mullite-based glass–ceramic glazes for floor tiles, Journal of Non-Crystalline Solids 352 (2006) 2159–2165.
[8] A. Escardino, J.L. Amoros, C. Feliu, J. Aparici, Study of crystalline phase formation in firing glazes based on the system SiO_2–CaO–MgO, in: 4th Conference of the European Ceramic Society (1995) 151–162
[9] G. Baldi, E. Generali, Effects of nucleating agents on diopside crystallization in new glass–ceramics for tile glaze application, Journal of Materials Science 30 (1995) 3251–3255.
[10] B. Eftekhari Yekta, P. Alizadeh, L. Rezazadeh, Floor tile glass–ceramic glaze for improvement of glaze surface properties, Journal of the European Ceramic Society 26 (2006) 3809–3812.
[11] A.M. Ferrari, L. Barbieri, C. Leonelli, C. Siligardi, Feasibility of using cordierite glass–ceramic as tile glazes, Journal of the American Ceramic Society 80 (1997) 1757–1766.

[12] F.J. Torres, J. Alarcón, Effect of MgO/CaO ratio on the microstructure of cordierite-based glass–ceramic glazes for floor tiles, Ceramics International 31 (2005) 683–690.
[13] F.J. Torres, E.R. de Sola, J. Alarcon, Effects of some additives on the development of spinel-based glass–ceramic glazes for floor tiles, Journal of Non-Crystalline Solids 351 (2005) 2453–2461.
[14] S. Banijamali, B. Eftekhari Yekta, H. Rezaie, V.K. Marghussian, Effect of fluorine content on sintering and crystallization behavior of CaO–Al_2O_3–SiO_2 glass–ceramic system, Advances in Applied Ceramics 107 (2008) 101–105.
[15] J.R. Taylor, A.C. Bull, Ceramics Glaze Technology, Pergamon Press, Oxford 34.
[16] S.M. Ohlberg, D.W. Strickler, Determination of percent crystallinity of partly devitrified glass by X-ray diffraction, Journal of the American Ceramic Society (1962) 170–171.
[17] ASTM International, Standard Test Method for Vickers Indentation Hardness of Advanced Ceramics, C 1328–08.
[18] E.M. Rabinovich, Review: preparation of glass by sintering, Journal of Materials Science 20 (1985) 4259–4297.
[19] W. Holand, G. Beall, M. Romero, Glass–Ceramic Technology, The American Ceramic Society, Ohio 111.